Study on Thermal-Mechanical Impact Effects on Parabolic Laser Thrusters

Zhiping Tang, Renping Xu, Jian Cai and Xiaojun Hu
Laser Propulsion Laboratory, Department of Modern Mechanics, University of Science and Technology of China, Hefei, China, 230026
zptang@ustc.edu.cn

Abstract

Thermal-mechanical impact failure problem of parabolic laser thrusters with air-breathing mode was studied experimentally and numerically. Four thermal loads i.e. the incident laser absorption, the radiation of high temperature gas, the transmitted laser absorption and the hot flow convection were proposed and the computational method of dynamic thermal-mechanical response of laser thruster was established. The calculated temperature rise of thrusters subjected to multiple laser pulses agreed well with the experimental measurement. The results show that for a parabolic thruster the thermal and mechanical damage mainly concentrates in the area near the apex and the mechanical fracturing will occur before melting. For a self-focus parabolic thruster the main temperature increase factors are the incident laser absorption and the high temperature gas radiation, while for an outside focus thruster, the main factor is the transmitted laser absorption near the apex. Thermal protection is needed for future laser thruster design.

NOMENCLATURE

q_i	Incident laser absorption power density
q_r	Absorption power density to high temperature gas radiation
q_t	Transmitted laser absorption power density
q_c	Convection heat power density
I	Incident laser power density,
α	Surface absorption coefficient,
θ	Angle
η	Transmission ratio through plasma,
T	Temperature
h	Heat transfer coefficient of flow convection
ρ	Density
u	Axial velocity
v	Radial velocity
p	Pressure
x	Radial coordinate
y	Axial coordinate
e	Specific internal energy,
β	Stress-temperature coefficient
ε_v	Volume strain,
c	Specific heat
K	Thermal diffusion coefficient
λ	Heat conductivity
E	Young's modulus
v	Poisson's ratio

1. INTRODUCTION

The primary principle of laser propulsion is applying a high temperature and high pressure plasma flow of propellant by absorbing pulsed laser energy to generate thrust. The instantaneous temperature in the central region of a plasma may reach over 10^4 K, which is much higher than the traditional chemical rocket engines. A laser thruster working in such environment for long time has to face severe thermal-mechanical impact. In 1998 Myrabo et al conducted a series of vertical propulsion tests of air-breathing mode with annular- focusing lightcrafts at the White Sand Missile Range, they found that when the flight height was beyond 30 m (4 s or 100 laser pulses) the thruster would melt or disintegrate in the air [1]. These tests fully demonstrated the severity of thermal-mechanical impact failure for laser propulsion. For future mission of launching micro-satellites into LEO, the laser power and launch time will be 10–100 times higher than that of Myrabo's tests, therefore, the thermal-mechanical impact will be one of the key problems in developing huge laser thrusters in the future.

The thermal-mechanical impact effects on target material induced by intensive laser pulse have been investigated for decades. Phipps et al [2] used to obtain the equations of parameters such as peak pressure etc on the target surface subjected to pulsed laser radiation. Cottet et al [3], Elizer et al [4] and Tang et al [5, 6] have reported the laser induced spall phenomena in metallic target plates which showed a strong shock fracture effect for intensive lasers. However, the study regarding thermal-mechanical impact failure mechanism in the field of laser propulsion is less reported. Tang et al [7] presented their numerical simulation for Myrabo's annular-focusing lightcraft. The results indicated that the main factors causing temperature increase were the transmitted laser absorption and the thermal radiation. The thruster structure will be disintegrated with partially fracture and melting at about 100 laser pulses. The computational prediction fitted the experimental observation well. An improved lightcraft model with ablation mode was also reported in Ref. [1], which created a world record flight height of 71 m, the reason was the solid propellant delrin blocked two main heat sources: the heat radiation and the transmitted laser energy to the wall near the focal point. Cai et al [8] have conducted the thermal-mechanical impact experiments for parabolic thrusters with ablation mode and measured the temperature increase and instantaneous pressure on the wall.

In this article, the thermal-mechanical impact phenomena for parabolic laser thrusters with air-breathing mode will be studied both experimentally and numerically. The motivation is to learn the failure mechanism and the main control factors for future thermal protection application.

2. TRANSMISSION OF FOCUSED LASER BEAMS IN THE AIR

Normally, a focused laser beam will break through the air to form plasma at the focus [9]. The plasma will absorb the energy of succeeding laser beam. We found an experimental phenomenon that a small iron ball behind the focus was moving and ablated as shown in Figure 1, which means there was still a partial energy of laser beam passing through the plasma and generating the thermal-mechanical action on the ball. To measure the transmission rate η, a Nd:YAG laser with pulse duration 20 ns and two laser energy meters by one in front of the focus and another behind the focus were applied in the experiment.

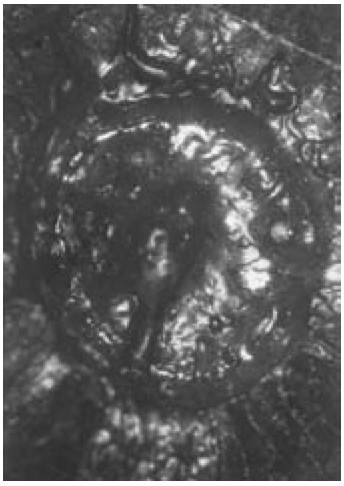

Figure 1. Photo of an iron ball ablated by the transmitted laser energy.

Table 1. Average transmission rate of laser beam with incident pulse energy

Experiments	E_i (J)	E_t (J)	η (%)
Set 1	7.1 ± 0.57	1.08 ± 0.5	14.7 ± 5.7
Set 2	9.7 ± 0.79	1.44 ± 0.53	14.5 ± 4.65
Set 3	12.7 ± 0.88	1.49 ± 0.71	11.5 ± 5

The pulse energy could be adjusted by setting the capacity voltage of the laser. Three sets of experiments were conducted with the pulse energy of 7 J, 10 J and 13 J, respectively, and each set had 5 shots. The experimental results are listed in Table 1 in which E_i, E_t are the average incident and transmitted laser energies, respectively. Due to the uncertainty of laser energy control and air breakdown point the experimental data have larger discreteness and error, however, Table 1 still shows that the average η decreases with the increase of incident energy.

3. THERMO-MECHANICAL IMPACT EXPERIMENTS FOR PARABOLIC THRUSTERS

3.1. Experimental setup

A TEA-CO_2 laser at Changchun Institute of Optical Machinery was used in the experiments. The wavelength of the laser was 10.6 μm, the pulse energy was 20 J, and the repetition rate could be adjusted from 66–150 Hz. The pulse duration was about 1 μs, but its main energy was concentrated within 200 ns. Figure 2 is a schematic of the experiments. Models A and B of parabolic thrusters were used in the study. Their geometry parameters are listed in Table 2. Models were made of aluminum alloy, the reflection coefficient of the inner wall was measured to be greater than 0.9. Three PVDF piezo-electric gauges G1, G2 and G3 were stuck on the inner wall for instantaneous pressure measurement. The locations of

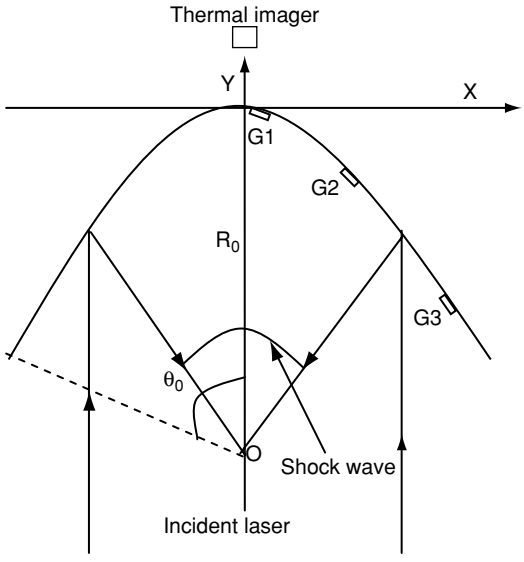

Figure 2. Schematic of pressure and temperature experiment.

Table 2. Parameters of parabolic thrusters*

Models	X_0(mm)	R_0(mm)	θ_0(°)	d(mm)	W(g)
A	25	5	136	0.25	2.1
B	32	10	116	1.5	16

* X_0 is the open end radius of the thruster, R_0 is the focal distance, θ_0 is the half angle as shown in Figure 2, d is the wall thickness, and w is the weight of the thruster.

G1, G2 and G3 at X-axis were 1.65, 11.54 and 18.50 mm for model A and 3.78, 9.89 and 25.23 mm for model B, respectively. The thickness of the gauges was 0.1 mm, and in the center of the gauge there was a PVDF piezo-electric sensor element of diameter 3 mm and thickness 28 μm.

The gauges were covered with an aluminum foil for thermal protection and reducing the influence of the wall reflection. The signals of 3 gauges were recorded by digital oscilloscopes. The temperature field of the outside wall was monitored by an infrared thermal imager TH51 of NEC company. Its measurement range was 0-200°C and the resolution was 0.2°C.

3.2. Results of temperature experiments

The temperature experiments were conducted with multi-pulse loading. 49 laser pulses were used for each experiment. The repetition rate was 66 Hz and the loading time was about 0.74 s. The thermal imager recorded the temperature field for more than 20 seconds with a speed of 1 frame/s. Figure 3 is a recorded image (with 512 × 512 pixels) for the thruster model A just after the laser pulse loading. It can be converted into the temperature distribution by the software attached with the imager. Figures 4 and 5 are the temperature – time curves of the outside wall at the locations corresponding to G1, G2 and G3 for thrusters A and B, respectively.

Figure 4 shows that for thruster A, all three locations reach the highest temperature at about 1 second after the end of laser loading and the temperature then decreases slowly. The highest temperature is 94.6ºC at the location of G1, which is near the apex. Figure 5 shows that the temperature increase of thruster B is much lower than that of thruster A. The highest temperature of thruster B at G1 location is only 48ºC and decays quickly. The reason is that the focal distance of Model B is twice of Model A and the wall of Model B is 5 times thick as Model A. Comparing two figures reveals that the

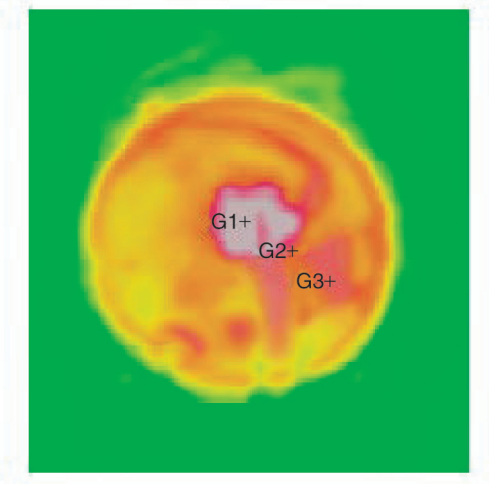

Figure 3. Recorded infrared image of thruster A at 1 s.

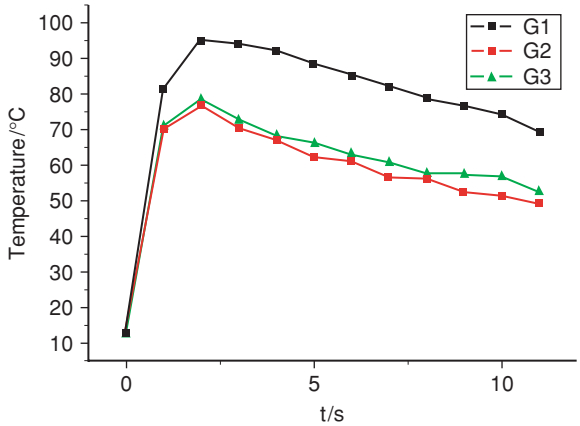

Figure 4. Temperature-time curves of thruster A.

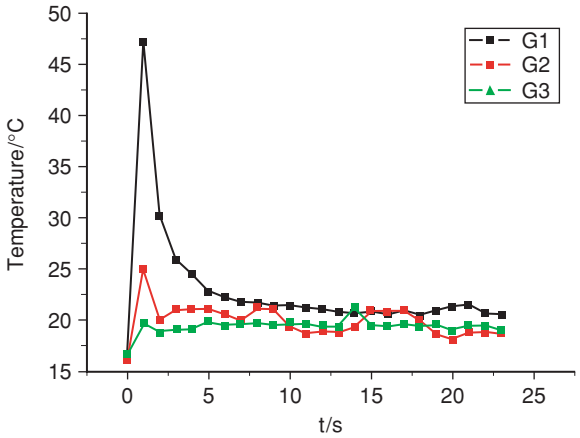

Figure 5. Temperature-time curves of thruster B.

temperature decay for Model A is much slower than that of Model B, which is due to the large half angle and deep focal point of Model A that can maintain the high temperature and high pressure gas for longer time in the thruster.

3.3. Pressure measurement on inner wall

Figures 6 and 7 are the measured inner wall pressure waveforms by PVDF gauges under a single laser pulse loading for thrusters A and B, respectively. Based on the recorded waveforms, the initial time of the laser pulse and the distance S from the gauge to the focal point the average shock wave speed V,

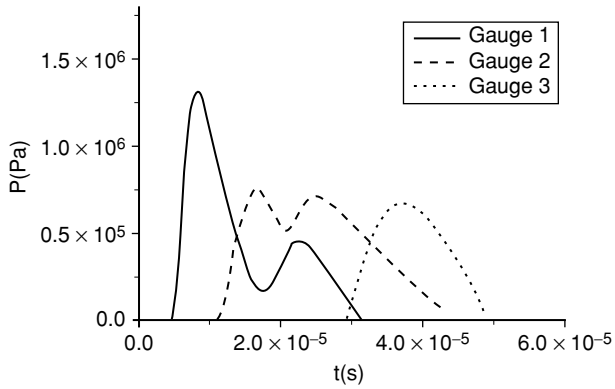

Figure 6. Pressure-time records of thruster A.

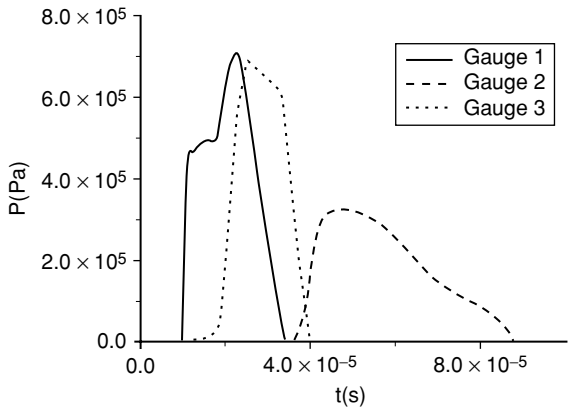

Figure 7. Pressure-time records of thruster B.

Table 3. Results of pressure measurement

	Thruster A			Thruster B		
Gauge	**G1**	**G2**	**G3**	**G1**	**G2**	**G3**
S (mm)	5.13	11.7	18.4	10.32	14.8	26
V (m/s)	1168	1114	620	1083	1049	730
p (MPa)	1.3	0.76	0.67	0.71	0.68	0.32
τ (μs)	27	32.5	49	24	26	50

the peak pressure p and the time duration τ of pressure can be calculated as listed in Table 3. The maximum pressure was 1.3Mpa at G1 of thruster A. The comparison between Figures 6 and 7 shows that the peak pressure and duration time of pressure at all gauge locations of thruster A are larger than that of thruster B, which is also related to the geometry of the thrusters.

3.4. Summary of experiments

Under laser loading with 49 pulses (66 Hz and 20 J/pulse), the highest temperature increase measured at outside wall was 80°C. Provided linear extrapolation the temperature will reach the melting temperature of aluminum alloy (660°C) after about 400 pulses or 6 seconds. Since the maximum impact pressure generated by laser pulse was 1.3 Mpa, the thruster should be damaged by the combined thermal-mechanical action before melting. Meanwhile, it was found that the inner wall finish became worse after several experiments, which could speed the damage process.

4. THERMAL LOADS, CONTROL EQUATIONS AND COMPUTATIONAL METHOD

4.1. Thermal loads for laser thruster

Normally the wall of a laser thruster will face 4 kinds of thermal loads under pulsed laser radiation [10]. They are the incident laser, the high temperature plasma heat radiation, the transmitted laser through plasma and the flow convection between hot gas flow and the wall.

4.1.1. Incident laser absorption

The incident laser absorption is defined as the direct absorption of the optical mirror surface to the incident laser beam. Eq. (1) gives the thermal power density q_i of the incident laser absorption

$$q_i = \alpha I \cos\theta \tag{1}$$

Where I is the incident laser power density, α is the surface absorption coefficient, θ is the angle between the laser beam and the normal line of the wall.

4.1.2. Heat radiation [10]

The high temperature and high pressure plasma can generate heat radiation. The absorption power density q_r of the thruster wall to such radiation can be described as

$$q_r = \int_{\sigma} \frac{J\alpha \cos\theta}{r^2} d\sigma \tag{2}$$

Where J is the radiation power of unit solid angle of plasma at a volume $d\sigma$, r is the distance between $d\sigma$ and the wall, θ is the angle between r and the normal direction of the wall, σ represents the radiation region of plasma.

4.1.3. Transmitted laser absorption

The focused incident laser beam may transmit partially through the plasma region and act directly on the wall as discussed in Section 2 previously, so the absorption power density of transmitted laser q_t will be

$$q_t = \alpha(1-\alpha)\eta(l_r/l_t)^2 I \cos\theta \tag{3}$$

Where η is the transmission ratio through the plasma, θ is the angle between the transmitted beam and the normal line of the wall, l_r and l_t are the distances of focus point to the reflection surface and the absorption surface, respectively.

4.1.4. Heat transfer by flow convection [10]

The high temperature gas flow contacts the inner wall and transfers heat to it. The convection heat power density q_c by a hot flow will be

$$q_c = h(T_s - T_f) \tag{4}$$

Where T_s is the wall temperature, T_f is the gas temperature, h is the heat transfer coefficient of flow convection.

4.2. Control equations

4.2.1. Flow equations

The flow equations for a 2D axial-symmetrical flow will be

$$\begin{cases} \left(\rho\right)_t + \left(\rho u\right)_x + \left(\rho v\right)_r + \dfrac{1}{2}\rho v = 0 \\ \left(\rho u\right)_t + \left(\rho u^2 + p\right)_x + \left(\rho uv\right)_r + \dfrac{1}{2}\rho uv = 0 \\ \left(\rho v\right)_t + \left(\rho uv\right)_x + \left(\rho v^2 + p\right)_r + \dfrac{1}{2}\rho v^2 = 0 \\ \left(e\right)_t + \left(eu + pu\right)_x + \left(ev + pv\right)_r + \dfrac{1}{2}\left(e + p\right)v = q \end{cases} \tag{5}$$

Where ρ, u, v, p are the density, axial velocity, radial velocity and pressure, respectively, y, x are the axial and radial coordinates, respectively, e is the specific internal energy, $e = \dfrac{1}{2}\rho\left(u^2 + v^2\right) + \dfrac{p}{\gamma - 1}$, in which γ is the adiabatic factor, and q is the absorbed laser energy of unit volume. Considering the high temperature ionization, γ and the specific heat were fitted with temperature based on the data base from 298 k to 500000 K [11] in the calculation to reflect the property of high temperature gas.

4.2.2. Control equations for thermal-mechanical impact calculation [12-14]

For a homogenous and isotropic thermal elastic object, its heat conduction equation and the initial and boundary conditions for element i can be derived based on the Fourier heat conduction law:

$$\beta T\frac{\partial \varepsilon_v}{\partial t} + \rho c\frac{\partial T}{\partial t} - K\left[\frac{\partial^2 T}{\partial x^2} + \frac{\partial T}{x\partial x} + \frac{\partial^2 T}{\partial y^2}\right] = 0 \tag{6}$$

$$\begin{cases} T\big|_{t=0} = T_0 & (r_i \le x_i \le R_i) \\ -\lambda\left(\dfrac{\partial T}{\partial x}\right)\Big|_{x_i = r_i} = q_i(t) + h\left[T(x_i, y_i, t) - f_i(t)\right] \end{cases} \tag{7}$$

Where x and y are the radial and axial coordinates of the thruster as shown in Figure 2, T is temperature, β is the stress-temperature coefficient, ε_v is volume strain, ρ is density, c is the specific heat, K is the thermal diffusion coefficient, λ is the heat conductivity, h is the heat transfer coefficient at surface. $f_i(t)$, $q_i(t)$ and $p_i(t)$ are the temperature, heat flow and pressure applying on the element i of the

wall, respectively. r_i and R_i are the radii of inner and outer surface of the wall element i, respectively.

The displacement equations and the initial and boundary conditions for an axial symmetric thermo-elastic dynamic problem will be

$$\begin{cases} \dfrac{E}{2(1+v)}\left(\dfrac{1}{1-2v}\dfrac{\partial \Theta}{\partial x}+\nabla^2 u_x-\dfrac{u_x}{x^2}\right)=\rho\dfrac{\partial^2 u_x}{\partial t^2}+\beta\dfrac{\partial T_i}{\partial x} \\ \dfrac{E}{2(1+v)}\left(\dfrac{1}{1-2v}\dfrac{\partial \Theta}{\partial y}+\nabla^2 u_y\right)=\rho\dfrac{\partial^2 u_y}{\partial t^2}+\beta\dfrac{\partial T_i}{\partial y} \end{cases} \tag{8}$$

$$\begin{cases} (u_x)_{t=0}=(\partial u_x/\partial x)_{t=0}=0 \\ (u_y)_{t=0}=(\partial u_y/\partial y)_{t=0}=0 \\ (u_x)_{x=0}=0 \\ \dfrac{E}{1+v}\left[\dfrac{(1-v)}{(1+v)}\dfrac{\partial u_x}{\partial x}+\dfrac{v}{(1-2v)}\dfrac{u_x}{x}+\dfrac{v}{(1-2v)}\dfrac{\partial u_y}{\partial y}-\beta T\right]_{x=r_i}=p_i(t) \end{cases} \tag{9}$$

Where $u_x(x_i, y_i, t)$ and $u_y(x_i, y_i, t)$ are the radial and axial displacements for element i, $\nabla^2=\partial^2/\partial x^2+(1/x)(\partial/\partial x)+\partial^2/\partial y^2$, $\Theta=\partial u_x/\partial x+u_x/x+\partial u_y/\partial y$ E is the Young's modulus and v is the Poisson's ratio.

4.3. Computational method

The calculation was divided into two parts: one for the unsteady flow and another for the thermo-mechanical impact of the thruster structure. The solid-fluid uncoupling method was applied for the latter, i.e. only the effect of the flow on the wall was considered in the computation. The calculation for unsteady plasma flow field was conducted by a commercial code FLUENT as done in References 15 and 16, which can offer the temperature and pressure distribution condition of the gas contacting with the wall. The thermal-mechanical impact response of the thruster was calculated by the code ABAQUS. A data treatment code which links two commercial codes was written by us.

5. CALCULATED RESULTS FOR PARABOLIC THRUSTER

The simulation was for the thruster model A. The cylindrical coordinate was applied as shown in Figure 2. The equation for the inner wall is $y = x^2/20$ (mm), and for the outside wall is $y = x^2/20.57 + 0.25$ (mm). The wall thickness is 0.25 mm. According to the geometry of a parabolic reflector the transmission is toward to the open end of the thruster after through the plasma at the focal point. Hence only the incident laser absorption, heat radiation and flow convection were taken into account in this simulation.

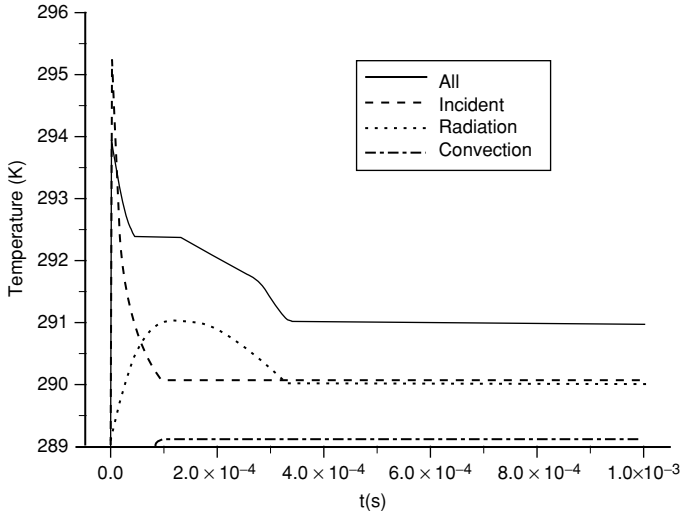

Figure 8. Calculated temperature-time curves for single pulse.

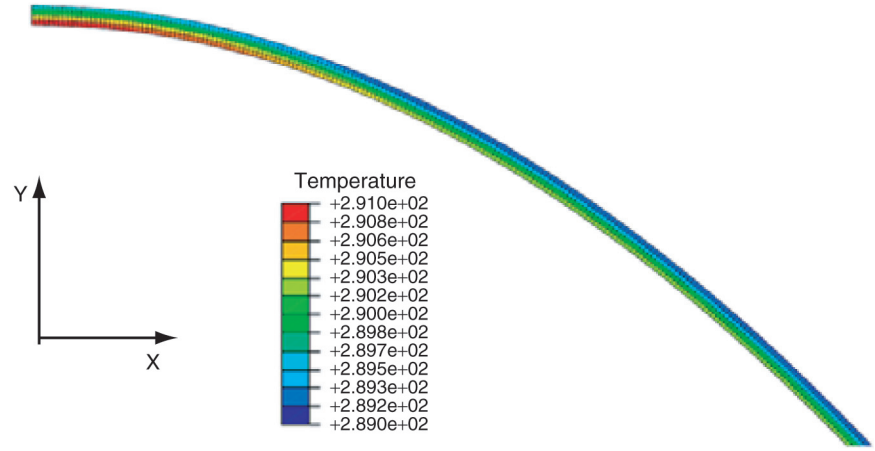

Figure 9. Calculated temperature distribution of the wall at 1 ms.

The radius of the incident laser beam was 25 mm and the energy distribution was assumed to be homogenous both in space and time. The material parameters of aluminum alloy used in computation are the density 2700 kg/m^3, the heat expansion coefficient 6.7 × 10^{-5} m^3/K, the heat conductivity 167 W/(m·K), the specific heat 896 J/kg·K, the Young's modulus 6.9 × 10^{10} pa and the Poisson's ratio 0.33 [17]. The initial temperature was 289 K. The surface absorption coefficient α was 0.05. Other experimental parameters are listed in Section 3.

5.1. Calculated results for single pulse

The pulse energy was 20 J, duration time was 1μs and the total time of the simulated process was 1ms. Figure 8 shows the temperature-time curves for three kind of thermal loads (incident laser absorption, heat radiation and flow convection) separately and combined, respectively. The curves are from the highest temperature point of the wall. Figure 9 shows the temperature distribution for the whole wall at 1ms. It can be observed from the figures that the incident laser absorption causes the temperature to increase and decrease rapidly since the laser pulse duration is only 1 μs. The action time of high temperature gas radiation is about 330 μs and the action time for flow convection is much longer. The temperature increments at 1 ms are 1.13 K, 1.00 K and 0.12 K for the incident laser absorption, high temperature radiation and flow convection, respectively. Under the combined heat loads the maximum temperature is 295.2 K at the apex but it decreases quickly. After the end of the hot gas radiation (330 μs) the temperature keeps steady. The temperature increment at 1 ms is 1.98 K located at x = 0.34 mm. Based on the single pulse simulation it reveals that the incident laser absorption and the high temperature gas radiation are the main factors of temperature increase and the flow convection can be neglected for a parabolic thruster using its inner surface as a mirror.

5.2. Calculation of multi-pulses

The laser energy was 20 J/pulse, frequency was 66 Hz and pulse number was 49. Figure 10 shows the temperature-time curves of outside wall at the locations of G1 and G2 after 49 pulses loading, in which the absorption coefficient α was 0.05 and 0.1 for Figures 10(a) and 10(b), respectively. The curves

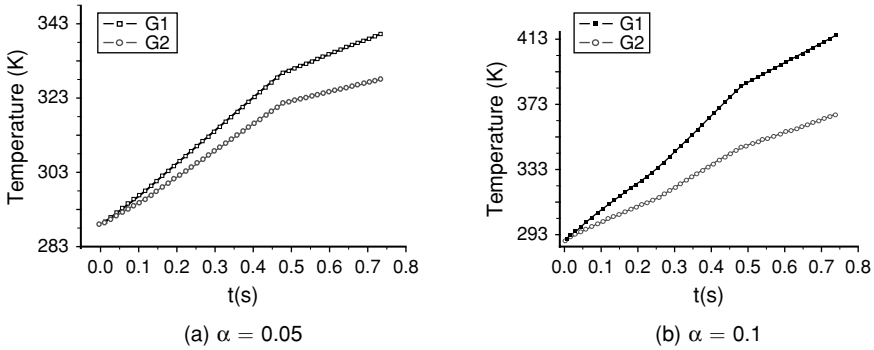

Figure 10. Temperature-time history of thruster A for multi-pulse loading.

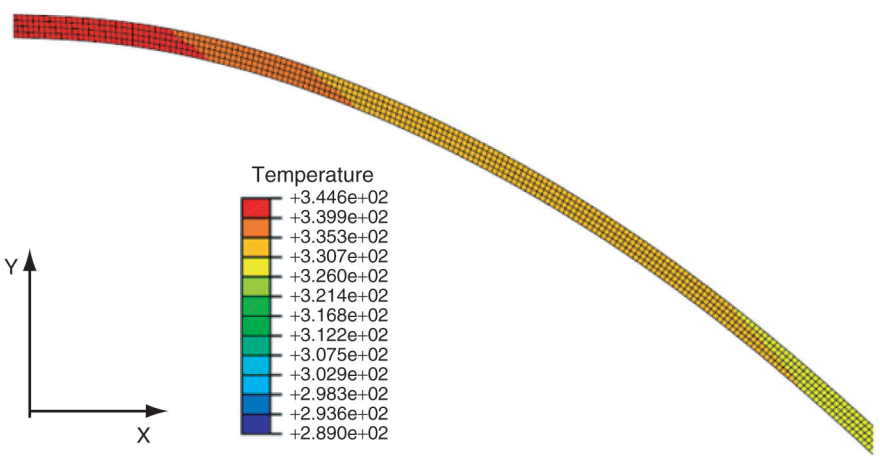

Figure 11. Temperature distribution of thruster A at 0.735 s for multi-pulse loading.

Table 4. Comparison of the calculated temperature increment to the experiment

Highest temperature increment (K)	G1	G2
Experimental	94.6	76.6
Calculated ($\alpha = 0.05$)	67.12	55
Calculated ($\alpha = 0.1$)	141.12	93.16

looks bi-linear and the inflection point appears at about 0.5 s (33 pulses). By analyzing the temperature distribution process the reason of inflection may be that at beginning the heat was deposited mainly on the region near the apex and transferred along the wall thickness, the temperature increases quickly, after that the effect of heat transfer along the wall surface direction became important too, which would slow down the temperature increase speed of apex region. Figure 11 shows the temperature distribution at 0.735 s (49 pulses). The maximum temperature is at the apex region and the temperature decreases along wall surface.

The highest temperature measured in the experiments appeared at 2 s instead of the end of laser load (0.735 s), the reason might be the delay of the instrument (the fastest speed of the thermal imager is 1image/s). The reflection performance of the inner surface of thruster A is not same, the measured average value was 0.9, some place it was 0.95. So in the simulation we took 2 absorption coefficients $\alpha = 0.05$ and $\alpha = 0.1$. Table 4 shows that for the maximum temperature increment the experimental data are between the calculated results of $\alpha = 0.05$ and $\alpha = 0.1$, which means the calculated result fit the

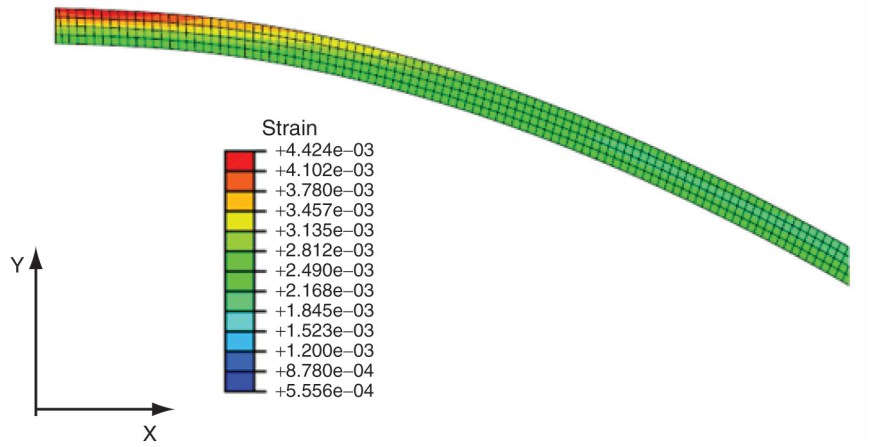

Figure 12. Calculated equivalent plastic strain distribution.

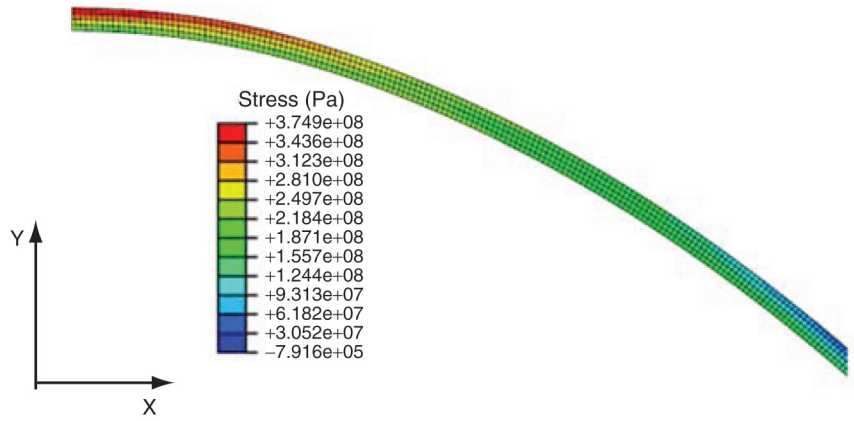

Figure 13. Calculated maximum tension stress distribution.

experimental one well. Also, the surface finish has great influence on the thermal response of the thruster. Along with the increase of the pulse number the optical performance will be getting worse, i.e. α will increase, which should be taken into account for further simulation.

5.3. Stress and strain calculation

Besides the thermal impact the wall of a laser thruster is subjected to cyclical mechanical impact of the pulsed flow. Figures 12 and 13 show the calculated equivalent plastic strain and the maximum tension stress distribution at the end of 49 pulses. The maximum tension stress and equivalent plastic strain appear at the outside surface at the apex region. There exits a region of tension stress beyond 300 Mpa. Although this stress is still below the tension strength at that temperature, along with the pulse number and temperature continuously increase the tension strength will decrease and finally the thruster structure will destroyed by the combined thermal and mechanical loading before melting, as predicted based on the experimental observation in Section 3.

6. THERMAL-MECHANICAL IMPACT UNDER MW POWER LASER LOADING

In future the laser power will be MW class, assuming the energy 10000 J/pulse, frequency 100 Hz and pulse duration 5 μs. The equation of the parabolic thruster is $x^2 = 0.08$ y, focal distance 0.02 m, the height is 0.125 m, the radius of the open end R_0 0.1 m and the wall thickness 2 mm. The material is aluminum alloy and $\alpha = 0.05$. Its weight is 300 g. The other parameters are the same as used in Section 5.

Figure 14 shows two focus modes. In Figure 14(a) the incident laser beam was focused by the inner surface (mirror) of the thruster, which we call it "Self-focus mode, SFM" while in Figure 14(b) the laser beam was focused by an outside lens or reflection mirror and we call it "outside-focus mode, OFM" in this article. In the previous sections only SFM was treated, A SFM thruster combines the optical mirror

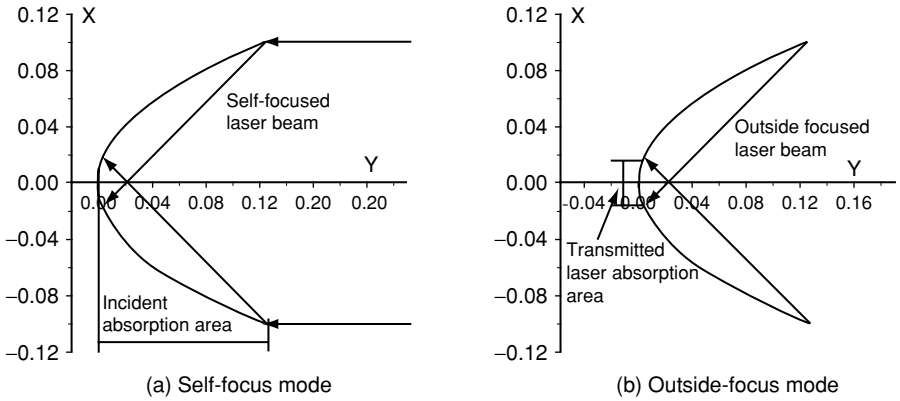

Figure 14. Two focus modes of thrusters.

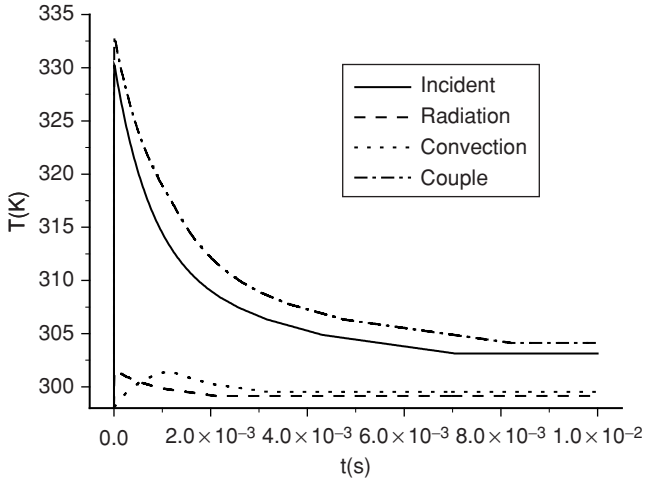

(a) Self-focus mode

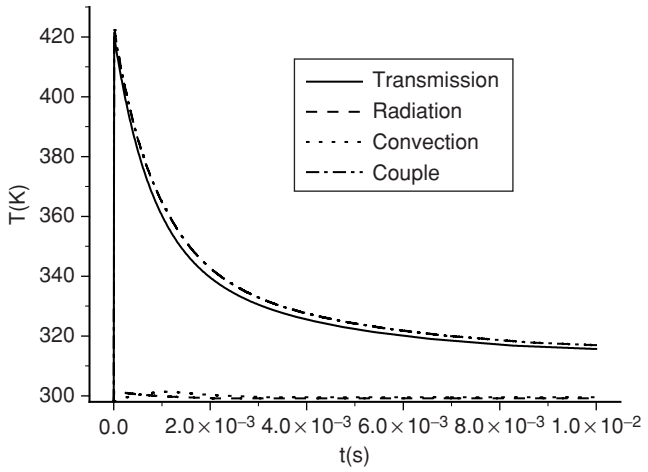

(b) Outside-focus mode

Figure 15. Temperature-time curves at apex of parabolic thrusters under single laser pulse.

and the thrust chamber into one while an OFM thruster separates them. The transmitted laser absorption for SFM and the incident laser absorption for OFM can be ignored in the simulation.

Figure 15 shows the temperature increase for two focus modes under single pulse load. The temperature increments of SFM at 10ms are 4.98 K, 0.98 K and 1.37 K for incident laser absorption, radiation and convection, respectively, while the temperature increments of OFM at 10ms are 17.51 K, 0.98 K and 1.37 K for transmitted laser absorption, radiation and convection, respectively. It can be seen that the main mechanism of temperature increase for a SFM thruster is the incident laser absorption which causes temperature increase of large area while the main mechanism of temperature increase for an Outside-focus thruster is the transmitted laser absorption which concentrates on the apex region and causes temperature increase of a small area.

Provided making a linear extrapolation based on the single pulse result, it will reach the thermal damage threshold and start to melt within about 100 pulses (1s) for a Self-focus thruster. Since its whole inner surface was exposed to the incident beam the thruster will melt with large area. For the Outside-focus mode the transmitted area near the apex of a thruster will reach thermal damage threshold at about 40 pulses (0.4 s) and then burn through a small hole. Hence, the thermal protection is necessary for MW class laser power and continuous propulsion. The calculation clarifies the main factors to prevent: The incident laser absorption for the Self-focus mode and the transmitted laser absorption for the Outside-focus mode.

The calculated maximum tension stress was 225 Mpa located at the apex for a single pulse load. The tension strength of aluminum alloy will be lower than 225 Mpa when the temperature exceeds 430 K

[17]. Hence, once the temperature increment of the thruster achieves 132 K (about 22 pulses for Self-focus mode or 8 pulses for Outside-focus mode) some elements will reach the tension damage threshold and produce cracks. It means the mechanical fracture appears before thermal melting which fits the conclusion in previous section. Along with the increase of temperature the thruster will be severely damaged under combined thermal and mechanical impact.

7. CONCLUSIONS

In this paper four thermal loads a parabolic laser thruster faces in air-breathing laser propulsion are introduced. They are incident laser absorption, heat radiation, transmitted laser absorption and flow convection.

The experimental and numerical results show that for a parabolic thruster the temperature increase and thermal damage (melt) mainly concentrates in the area near the apex. The mechanical impact comes from the shock waves and moving fluid in plasma flow induced by the pulsed laser. Along with the increase of temperature the mechanical micro cracks will occur first near the apex before thermal melt. The combined thermal and mechanical action speeds the process of fracturing, melting and disintegrating.

The numerical simulation reveals the thermal absorption mechanisms. For a self-focus parabolic thruster the main temperature increase factors are the incident laser absorption and the high temperature gas radiation, the latter is inverse proportional to the square of the focal distance. While for an outside focus thruster, the main factor of temperature increase is the transmitted laser absorption which causes the severe thermal impact near the apex.

The present study has shown that the thermal protection is needed for future laser thruster design and the main thermal absorption mechanisms can be a reference for the design.

REFERENCES

[1] Myrabo L. N., World record flights of beam-riding rocket lightcraft - Demonstration of disruptive propulsion technology, AIAA-2001-3798, 2001.

[2] Phipps C R, Turner Jr T P, et al, Impulse coupling to targets in vacuum by KrF, HF, and CO_2 single-pulse lasers, *J. Appl. Phys*., Vol. 64 , 1988, pp. 1083–1096.

[3] Cottet F. and Boustie M, Spallation studies in aluminum targets using shock waves induced by laser irradiation at various pulse durations, *J Appl Phys*., Vol. 66, 1989, pp. 4067–4073.

[4] Eliezer S. and Gilath I, Laser-induced spall in metals: Experiment and simulation, *J Appl Phys.,* Vol. 67, 1990, pp. 715–724.

[5] Tang Z P, Li X Z, Zhou G Q, Liao X L, et al, Experimental investigation of laser-induced spall in metallic targets, *Chinese Sci. Bulletin*, Vol. 38, 1993, pp. 781–784.

[6] Tang Z P, Zhou G Q and Li X Z, Laser-induced spalling in aluminum and the analytical model, in *Proc. of 2nd ISIDE*, Sichuan Univ. Press, Chengdu, 1992, pp. 598–602.

[7] Tang Z P and Xu R P, Numerical Study On Thermal-Mechanical Impact Failure Mechanism For Annular-Focusing Laser Thrusters, in *Proc. of ISBEP-6*, 2009, USA.

[8] Cai J, Hu X J, Tang Z P, and Li L, Experimental study of laser propulsion with ablation mode, *Chinese J. of Propulsion Technology*, Vol. 29, 2008, pp. 371–376.

[9] Musal H M, "Pulsed Laser Initiation of Surface Plasma on Metal Mirrors", in *Laser Induced Damage In Optical Materials: 1980*, edited by H.E. Bennett et al., NBS Special Publication 620, NBS, Boulder, Colorado, 1981, p. 227.

[10] Bian Y G and Xu L G, *Gas Thermodynamics*, Press of the Univ. of Science and Technology of China, 1997, Hefei, China.

[11] Zel'dovich Y B and Raizer Y P, *Physics of Shock Waves and High-Temperature Hydrodynamic Phenomena*, Science Press, Beijing, 1980 (Chinese translation edition).

[12] Sun C W, *The effects of laser radiation*, Press of Defense Industry, Beijing, 2002.

[13] Lu M W and Luo X F, *The foundation of elastic theory*, Press of Tsinhua Univ., Beijing, 1997.

[14] Ding S, Wang J G, Wang Y H and Liu F, Similarity of thermal-mechanical coupling under laser radiation, *Intensive Lasers and Particle beams*, Vol. 17, 2005, pp. 1331–1334.

[15] Ping G and Tang Z P, Numerical Simulation for Laser Propulsion of Air Breathing Mode Considering Moving Boundaries and Multi-Pulses, *Beamed Energy Propulsion: Fourth International Symposium on Beamed Energy Propulsion*. 2006, pp. 87–94.

[16] Xu R P and Tang Z P, Numerical simulation of multi-pulse laser propulsion with air-breathing mode, *Intensive Lasers and Particle Beams*, Vol. 19, 2007, pp. 369–372.

[17] Wang Z T and Tian R Z, *Handbook of Aluminum Alloys and Manufactory*, Press of South Central Univ., 2005.